

# Statistical isotropy violation in WMAP CMB maps due to non-circular beams

Santanu Das, Sanjit Mitra, Aditya Rotti, Nidhi Pant, and, Tarun Souradeep

santanud@iucaa.ernet.in, sanjit@iucaa.ernet.in, aditya@iucaa.ernet.in,

nidhip@iucaa.ernet.in, tarun@iucaa.ernet.in

IUCAA, P. O. Bag 4, Ganeshkhind, Pune 411007, India

## ABSTRACT

Statistical isotropy (SI) of Cosmic Microwave Background (CMB) fluctuations is a key observational test to validate the cosmological principle underlying the standard model of cosmology. While a detection of SI violation would have immense cosmological ramification, it is important to recognize their possible origin in systematic effects of observations. WMAP-7 release claimed significant deviation from statistical isotropy (SI) in the bipolar spherical harmonic (BipoSH) coefficients  $A_{ll}^{20}$  and  $A_{l-2l}^{20}$ . We simulate CMB maps using actual WMAP non-circular beams and scanning strategy. Our estimated BipoSH spectra from these maps match the WMAP-7 results very well. This is the first explicit and conclusive demonstration that the SI violation reported in WMAP-7 maps is due to the non-circularity of the beams. It is also evident that only a very careful and adequately detailed modeling, as carried out here, can conclusively establish that the entire signal arises from non-circular beam effect. This is important since cosmic SI violation signals are expected to be subtle and dismissing a large SI violation signal as observational artefact based on simplistic ‘plausibility’ arguments run the serious risk of throwing the ‘baby with the bathwater’.

CMB measurements have spearheaded the transition of cosmology to a precision science. The recent observations by WMAP and Planck favour a minimal six parameter  $\Lambda$ CDM cosmology (Hinshaw et al. 2013; Planck Collaboration et al. 2013a). Assumption of statistical isotropy (SI) of CMB is a fundamental tenet of the standard model of cosmology, that the increasingly exquisite precision of measurements now allow to be observationally tested. Indeed several SI anomalies have been detected in recent measurements of CMB temperature anisotropies (Bennett et al. 2013; Bennett et al. 2011; Planck Collaboration et al. 2013b). Though there is no dearth of proposed theoretical models (Ackerman et al. 2007; Pullen & Kamionkowski 2007; Rotti et al. 2011) to explain these SI violations, it is imperative to model all the known systematics and account for the biases introduced by them before probing any deeper for subtle cosmological effects.

It is well known that, non-circular instrumental beams can induce artefacts in CMB measurements. The resultant effect on CMB angular power spectrum has been extensively studied in literature (Tegmark et al. 2003; M. A. J. Ashdown et al. 2007; Fosalba et al. 2002; Hinshaw et al. 2007; Mitra et al. 2009, 2004; Souradeep et al. 2006; Souradeep & Ratra 2001; Das & Souradeep 2013). It was recognized that non-circular beams can lead to SI violation in the observed maps not captured in the angular power spectrum (Hajian & Souradeep 2003; Mitra et al. 2004). Bipolar spherical harmonic (BipoSH) expansion of the CMB two point correlation function provides a novel tool to probe SI violation in CMB maps (Hajian & Souradeep 2003). Detection of non-zero BipoSH spectra,  $A_{l_1 l_2}^{LM}$  ( $L > 0$ ), is the basic probe of SI violation.

In this work we address the high statistical significance detection of SI violation by the WMAP-

7 team in BipoSH coefficients  $A_{ll}^{20}$  and  $A_{l-2l}^{20}$  from the WMAP “V” and “W” band maps (Bennett et al. 2011). In a recent paper, we provided a formalism to study non-circular beams in BipoSH representation and show that mild non-circularity at levels comparable to WMAP beams do generate significant BipoSH spectra in observed CMB maps (Joshi et al. 2012). This was also indicated in a work that approximately modelled the non-circular beam effect in terms of anisotropic power spectrum (Hanson et al. 2010). However, given the strong SI violation signal, it is important to establish that this signal solely arises from non-circular beam effects. Ascribing origin in systematic effect based incomplete assessment runs the risk of missing interesting coexistent SI violation signal.

Estimating the full systematic effect, by incorporating the complex structure of the actual experimental beam along with non-trivial scan strategy, necessitates detailed numerical simulations. In this paper, we simulate (observed) CMB sky maps by combining actual WMAP instrumental beams with the scan strategies for “V” and “W” band instruments. The BipoSH spectra obtained from these maps match the spectra recovered by an identical analysis on WMAP-7 observed maps. This is the first time it has been convincingly established, via explicit matching of the recovered BipoSH spectra, that non-circular beams caused the WMAP-7 quadrupolar anomaly.

## 1. Review of BipoSH

The standard model of cosmology assumes the universe to be SI. The CMB temperature anisotropies can be expressed in terms of the spherical harmonics as

$$T(\hat{n}) = \sum_{l=0}^{\infty} \sum_{m=-l}^l a_{lm} Y_{lm}(\hat{n}), \quad (1)$$

where  $a_{lm}$  are the coefficients of expansion in this basis. If the CMB temperature anisotropies are described as a Gaussian random field, warranted by recent precise measurements made by PLANCK (Planck Collaboration et al. 2013b,c), specifying the two-point correlation for this field completely characterises its statistical properties. Further, if the basic assumption of SI is valid, then the two point correlation function is fully described by the equivalent harmonic space quantity,

the angular power spectrum  $C_\ell$  defined as

$$\langle a_{lm} a_{l'm'}^* \rangle = C_l \delta_{ll'} \delta_{mm'}, \quad (2)$$

where the angular brackets  $\langle \dots \rangle$  denotes an average over an ensemble of CMB realizations.

However, if the assumption of SI is not valid,  $C_\ell$  alone does not provide a complete statistical description of the CMB temperature anisotropies. In a non-SI universe, it is necessary to specify the angular power spectrum as well as the BipoSH coefficients, which are set of spectra which encode the information of the direction dependent part of the two-point correlation function (Hajian & Souradeep 2003). The BipoSH spectra  $A_{ll'}^{LM}$  are given by the following expression,

$$\langle a_{lm} a_{l'm'}^* \rangle = \sum_{LM} \mathcal{C}_{lml'm'}^{LM} A_{ll'}^{LM}, \quad (3)$$

where  $\mathcal{C}_{lml'm'}^{LM}$  are the Clebsch-Gordan coefficients.

The BipoSH spectra are a generalization to the the angular power spectra. The subset of BipoSH spectra  $A_{ll}^{00} = (-1)^l \sqrt{2l+1} C_l$  are equivalent to the angular spectrum, while the remaining set of BipoSH spectra quantify SI violation. Measuring non-vanishing power in the BipoSH spectra  $A_{ll'}^{LM}$ ,  $L, M \neq 0$  forms the basic criteria of searching for deviations from SI.

## 2. Simulation and Analysis

The WMAP satellite scanned the sky temperature in five different frequency bands at 22, 30, 40, 60 and 90 GHz, named as “K”, “Ka”, “Q”, “V” and “W” respectively. WMAP-7 team searched for SI violation signals in the “V” and the “W” bands, since these so called CMB channels are the least foreground contaminated and detected significant non-vanishing BipoSH spectra  $A_{ll}^{20}$  and  $A_{l-2l}^{20}$ . We simulate observed CMB maps, by closely replicating the WMAP instrument characteristics and scanning strategy for the same bands.

The “V” band has two detectors and the “W” band comprises of four detectors. Since each detector has its unique beam pattern and scan path, it is important to carry out the simulations for each differencing assembly (DA) independently. We generate 30 realisations of SI CMB skies from the best fit WMAP-7 angular power spectrum using HEALPix (Gorski et al. 2005). Thereafter,

these maps are scanned using the WMAP scan pattern and convolved with the beam functions of each DA. This results in time order data (TOD) for each DA, from which the observed maps are reconstructed using a map-making algorithm. The details of all these simulation procedure are discussed below.

### Scan pattern

Each of the DA of WMAP satellite is equipped with a pair of radiometers. WMAP satellite during scanning the sky measures the temperature difference between its two antennas of each of the DA. Each of these antennas are roughly inclined at an angle  $70.5^\circ$  with the symmetry axis of the satellite. The satellite spins around its main axis with a period of 2.2 min and slowly precesses about the Sun-Earth axis at an inclination angle of  $22.5^\circ$ , with precession period of about an hour. This particular method of scanning is adapted by WMAP to reduce noise in the data. This entire system is located at L2 and is moving around the Sun with a period of one year.

We have used an analytical approximation (Das & Souradeep 2013; Moss et al. 2011) to calculate the position of the two horns of the satellite as a function of time. This allows us to get the beam locations and their orientations on the sky.

### Beam functions

The observed temperature  $T(\hat{n})$  along a particular direction  $\hat{n}$  is related to the underlying sky temperature  $\tilde{T}(\hat{n})$  by the following expression,

$$T(\hat{n}) = \int B(\hat{n}, \hat{n}') \tilde{T}(\hat{n}') d\Omega_{\hat{n}'}, \quad (4)$$

where  $B(\hat{n}, \hat{n}')$  is the beam response function. To give the reader a sense for the shape and size of the intrinsic instrumental beams, if elliptical Gaussian (EG) profiles are fitted to WMAP beams, the FWHM of W band beam will be  $\sim 13.2'$  and eccentricity  $\sim 0.4$ , and the FWHM of V band will be  $\sim 21.0'$  and the eccentricity 0.46 (Jarosik et al. 2007; Mitra et al. 2004). This however does not include the effect of scanning, which creates varying effective beam profile across the sky (Mitra et al. 2011). These elliptical Gaussian approximations of the beam profiles *do not provide adequate accuracy* for high-precision CMB analysis. Likewise, while evaluating BipoSH coefficients, such an

approximation is no longer valid, as it can not explain subtle features generated due to non-circular beam (Joshi et al. 2012). Therefore, a full convolution of SI CMB sky with the actual beam along with scanning strategy of WMAP is important for checking the effect on BipoSH spectra.

WMAP beam maps are available as a  $600 \times 600$  array on the LAMBDA website<sup>1</sup>. Each side of this array represents  $24^\circ$  of the beam and thus each of these pixels covers  $2.2'$  of the beam profile. Apart from the central peak, the beam consists of many small structures around the peak, as seen in Fig. 1, which span a much wider solid angle. This includes sub-dominant side peaks and a noisy annular region, which is significant up to  $\sim 4^\circ$  radial distance from the central peak. Note that the noisy part of the beam consists of many points where the beam response function is negative (see Fig. 1), which later on shows up as changes in sign of BipoSH spectra for V band in WMAP-7 year observations (Joshi et al. 2012). The noisy annular region cannot be ignored even though the sensitivity of the central part of the beam is very high, because this region spreads over a really large region. In effect, the total sensitivity of the negative annular region of the beam is comparable to the sensitivity of the central Gaussian peak. Another important fact to notice in the beam profile is that the negative region of the beam contributes to approximately 50% of the total beam sensitivity. Realistically, it is important to consider the entire annular part of the beam. In our analysis, we have taken  $6^\circ$  radial cut-off for the beam while numerically convolving it with the sky map using Eq. (5). We have tested that ignoring the part beyond  $6^\circ$  does not affect our results.

### Generation of Time Ordered Data

On the observed pixelated sky map, the convolution equation will also have to discretised. Then the measured sky temperature along a given direction  $\hat{n}$  can be expressed as,

$$T(\hat{n}) = \frac{\sum_{i \in S_{\hat{n}}} B(\hat{n}'_i, \hat{n}) \tilde{T}(\hat{n}'_i)}{\sum_{i \in S_{\hat{n}}} B(\hat{n}'_i, \hat{n})}, \quad (5)$$

<sup>1</sup>[http://lambda.gsfc.nasa.gov/product/map/dr5/beam\\_maps\\_get.cfm](http://lambda.gsfc.nasa.gov/product/map/dr5/beam_maps_get.cfm)

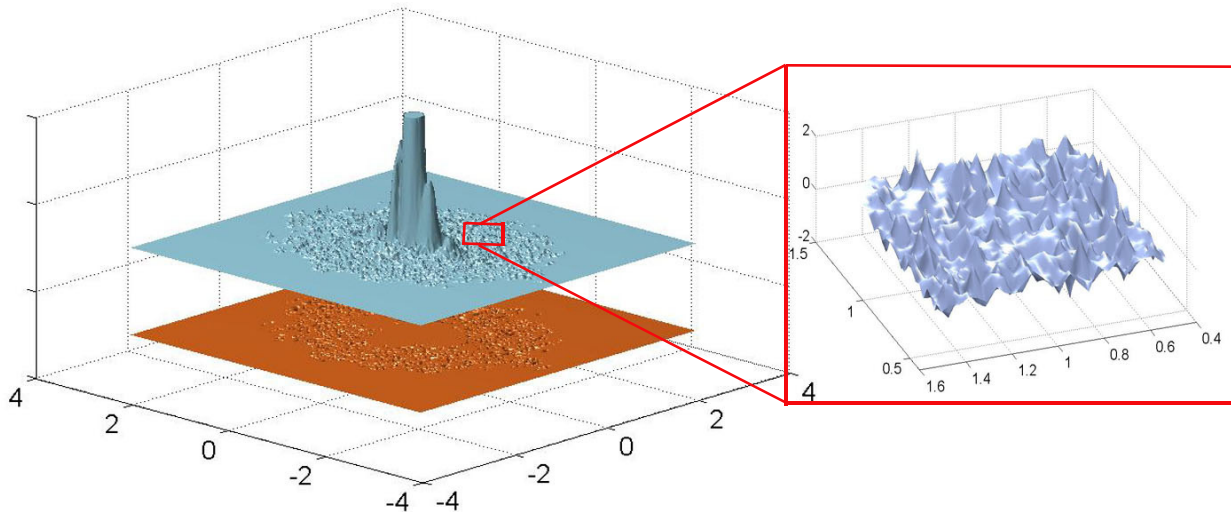


Fig. 1.— The figure shows an enlarged view of A side beam of W3 DA. The central part of the beam is truncated to show the sub-dominant structures in the beam. Apart from the central peak the beam consists of many features extending up to  $\pm 3$  degree in an annular ring. There are many pixels in the annular region where the value of the beam goes negative. Visually, we have separated the negative (blue) and positive (orange) sensitivity part to show their respective spreads. A small portion with positive sensitivity of the beam is enlarged to show the several features present in the beam. These seemingly negligible fluctuations contribute significantly to SI violation and hence must be included with every detail in the convolution process. Specifically, our study shows that the negatives in these fluctuations are critical for explaining the zero crossing in the BipoSH spectra.

where  $S_{\hat{n}}$  is the set of all the pixels for which  $B(\hat{n}'_i, \hat{n})$ , is non-zero for a pointing direction  $\hat{n}$  and  $\hat{n}'_i$  is the central direction of the pixel. If the beam function is considered to be elliptical Gaussian, then pixels within  $3-4\sigma$  would have been sufficient for the numerical integration. However, the actual WMAP beams, as shown in Fig. 1, where we have plotted the beam map of A side of W3 DA, this area cut-off is not valid and requires integration over the entire beam.

For calculating the observed temperature along a direction [see Eq.(5)], we include all the pixels inside the radius  $\pm 6^\circ$ , from that particular direction and then interpolate the beam function at the center of the pixels. Thereafter, we multiply this beam function with the temperature and then sum over all the included pixels. WMAP team provides the temperature sky maps at  $N_{side} = 512$ . At this resolution, the distance between two adjacent pixel centres is  $3.8'$ . As the sizes of many of the noisy peaks in the skirt of the beams are smaller than  $3.8'$ , these features will be missed in

numerical integration, hence the convolution will not be precise. To overcome this problem, all the simulations in the paper are generated at a resolution  $N_{side} = 1024$ , for accurate evaluation of the numerical beam convolution of the map, following which the pointing direction is converted to the pixel numbers corresponding to  $N_{side} = 512$  resolution map.

In order to get the value of the beam function at the center of each pixel, it is necessary to use a fast and accurate interpolation scheme. Linear interpolation to the centre of each pixel by considering the value of the beam function at the four pixels around only works for the central peak. However, the noisy features in the annular region surrounding the central peak of the beams being highly fluctuating, the error due to linear interpolation is found to be unacceptably large. In this region, a non-linear interpolation schemes, such as the cubic or the spline interpolation, may provide reasonable results. But these methods are computationally expensive. To overcome this issue, we

upgrade the beam function from  $600 \times 600$  grid to  $2400 \times 2400$  grid using MATLAB's `spline2` interpolation scheme. This high resolution grid enables us to use linear interpolation of the beam in the convolution process without compromising precision and being computationally fast. We have also checked that further increment in the interpolated grid size is not required for improving accuracy.

### Map-making

Numerical implementation of the above procedure results in the generation of the time ordered data, where each sample is obtained by Eq. (5). The time-ordered data (TOD) vector for each DA can then be written as,

$$d = AT + N, \quad (6)$$

where  $T$  is the scanned sky temperature,  $A$  is the pointing matrix and  $N$  is the instrumental noise. We have not considered any noise in our analysis and therefore  $N = 0$ . Since, WMAP follows a differential scan pattern, each of the row of the pointing matrix consists of one +1 one -1 and all other components of the matrix are zero. The temperature can be estimated from the time order data (TOD) as,

$$\bar{T} = (A^T A)^{-1} A^T d. \quad (7)$$

It is not possible to invert the matrix in a brute force way as the size of the matrix is huge,  $N_{pix} \times N_{pix}$ , where  $N_{pix} \sim 3 \times 10^6$ , is total number of pixels in the map. Different numerical method for map-making has been discussed in (Hamilton 2003; Das & Souradeep 2013). In this paper, we have used the Jacobi iteration method, details of which has been discussed in (Das & Souradeep 2013).

### BipoSH analysis in presence of masks

The observed CMB maps are contaminated by foregrounds. Even though the W and V band maps are the least foreground contaminated, the region close to the galactic equator have to be masked to extract information on the genuine CMB signal. Application of masks in analyses as well as presence of anisotropic noise in the maps, correlates different harmonic modes of CMB anisotropies and introduces SI violation, which lead to non vanishing BipoSH spectra. To remove this bias from observed WMAP maps masked

with KQ-75, firstly we evaluate BipoSH coefficients from 1000 masked realisations generated from `synfast` subroutine of HEALPix for the best fit CMB power spectrum, average beam transfer function and anisotropic noise model (Rotti et al. 2011). This estimate is used to debias and arrive at the final WMAP BipoSH spectra  $A_{ll}^{20}$  and  $A_{l-2l}^{20}$ . These results closely resemble to WMAP findings. The differences are essentially due to differences in methodology.

We now apply our WMAP analysis on our simulated maps with non-circular beam and scan strategy. We perform an identical BipoSH analysis on these maps. Even though we do not include foregrounds in our simulations, we use the mask in our analysis, in order to mimic the actual conditions.

### 3. Results

WMAP-7 team detected a SI violation signal in BipoSH spectra both in the “V” and the “W” bands. The primary goal of this paper is to make a detailed computation of the BipoSH spectra arising from the actual WMAP beam coupled to the scan strategy and establish conclusively that the measured non-zero  $L = 2$  BipoSH spectra in WMAP-7 can be entirely attributed to this systematic effect. We generate 30 simulations each for four DAs in W band (W1, W2, W3, W4) and two DAs in V band (V1, V2) by convolving CMB sky realisations with actual WMAP beam and scanning strategy and performed BipoSH analysis on each set separately. The BipoSH spectra obtained from the true and simulated datasets are shown in Fig. 2.

In Fig. 2 we have plotted the WMAP data points using the red errorbars. These errorbars are derived from 1000 simulations used for estimating the mask bias. The average  $A_{ll'}^{LM}$ s from the four DAs are plotted in black dashed lines. It can be seen that the BipoSH spectra of simulated maps match well with the results obtained from our analysis on the WMAP-7 observed maps. Specifically, the location of the peaks of the BipoSH spectra and the “zero crossings” caused by the negative values of the beam are very well recovered. The errorbars are not plotted for each individual DA to avoid clutter in the plot, rather we have plotted the errorbars of the average spectra. We have plotted two errorbars, the regions shaded



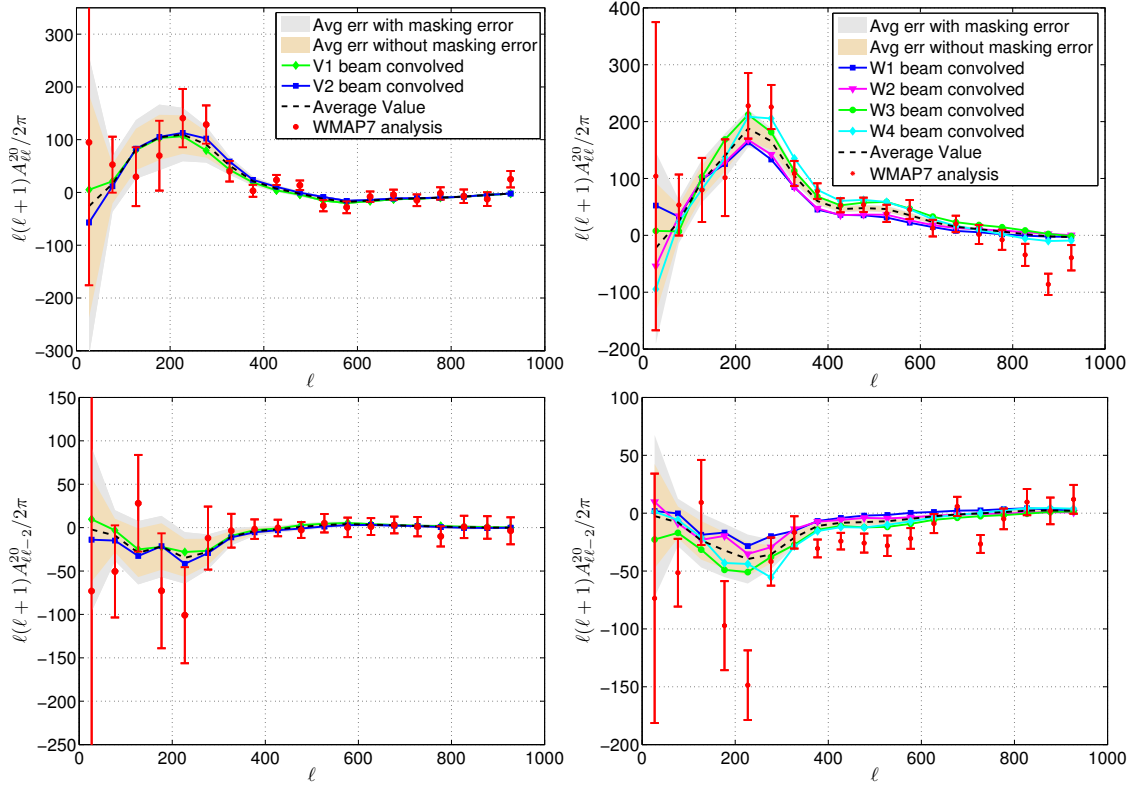


Fig. 2.— We present a comparison between the BipSH spectra  $A_{\ell\ell}^{20}$  (top panels) and  $A_{\ell\ell-2}^{20}$  (bottom panels) obtained from WMAP maps (red errorbars), observed in V (left panels) and W (right panels) bands, and our detailed simulations of the respective channels (solid lines). The average BipSH spectra across the DAs are denoted by the dashed lines. The saffron band shows the standard error derived from all the simulations for each band only (total 60 for V and 120 for W), while the grey band also combines the error on the mask bias correction. The location of peak of the  $A_{\ell\ell}^{20}$  spectra is set by both the first CMB acoustic peak, and the beam-width. A closer inspection of the  $A_{\ell\ell}^{20}$  spectrum reveals a change in sign, seen for both the bands, which can only be explained by the negatives in the beam function, as seen in Fig. 1. Thus the spectra from the simulated maps match the observed spectra very well, replicating the non-trivial features, leaving very little scope for accommodating other systematic or cosmological effects to explain these observations.

in orange denote standard errors estimated from the DA simulations alone, while in the grey region we also include the standard errors on the mask bias in quadrature. The error seen at high- $\ell$  in the WMAP analysis is mostly due to noise in the simulations used for mask bias subtraction. Since we do not include noise in the DA simulations, the corresponding errorbars are small.

For W-band, it can be seen in the figure that BipSH spectra for W1 and W2 are very close to each other and similarly for W3 and W4. This trend is essentially due to similarities in their respective beam transfer functions.

#### 4. Discussion and conclusion

In this letter, we have demonstrated for the first time that the quadrupole anomaly seen in WMAP-7 maps can be completely explained by incorporating the effect of non-circular beams and scan strategy of the satellite. This clearly indicates that this signal does not have any cosmological origin. The absence of similar detections in BipSH spectra  $A_{\ell\ell}^{20}$  and  $A_{\ell\ell-2}^{20}$  in the more recent measurements by the Planck satellite (Planck Collaboration et al. 2013b) reinforces this claim. Prior to that WMAP-9 team released a set of

non-circular beam deconvolved maps, which also did not show this particular SI violation signature, however, the deconvolution procedure renders the resultant maps unsuitable for cosmology analyses (Bennett et al. 2013). The work presented here demonstrates that detailed numerical methods allow the subtraction of these systematic biases accurately.

In order to improve the accuracy of this analysis, it may be necessary to include foreground models and anisotropic noise in the simulations. It may also be important to incorporate the coupling between beam and mask, which has been neglected in this paper while correcting for the mask bias. This, in turn, will enable one to probe SI violation sourced by deviations from the standard model of cosmology or other subtle late time effects, like weak lensing, which will be targeted by the current and upcoming CMB missions.

## 5. Acknowledgements

We would like to thank Saurabh Kumar, Gary Hinshaw and Eiichiro Komatsu for useful comments and help. SD and AR acknowledge the Council of Scientific and Industrial Research (CSIR), India for financial support through Senior Research Fellowships. SM acknowledges the support of Department of Science and Technology (DST), India for the SERB FastTrack grant SR/FTP/PS-030/2012. TS acknowledges Swarnajayanti fellowship grant of DST India. Computations were carried out at the HPC facilities at IUCAA.

## REFERENCES

- Ackerman, L., Carroll, S. M., & Wise, M. B. 2007, *Physical Review D*, 75, 083502
- Bennett, C. L., Hill, R. S., Hinshaw, G., et al. 2011, *Astrophys. J. Supplement Series*, 192, 19
- Bennett, C. L., Larson, D., Weiland, J. L., et al. 2013, *ApJS*, 208, 20
- Das, S., & Souradeep, T. 2013, arXiv:1307.0001
- Fosalba, P., Doré, O., & Bouchet, F. R. 2002, *Phys. Rev. D*, 65, 063003
- Gorski, K. M., Hivon, E., Banday, A. J., et al. 2005, *Astrophysical Journal*, 622, 759
- Hajian, A., & Souradeep, T. 2003, *Astrophysical Journal Letters*, 597, L5
- Hamilton, J. . 2003, astro-ph/0310787
- Hanson, D., Lewis, A., & Challinor, A. 2010, *Phys. Rev. D*, 81, 103003
- Hinshaw, G., Nolta, M. R., Bennett, C. L., et al. 2007, *ApJS*, 170, 288
- Hinshaw, G., Larson, D., Komatsu, E., et al. 2013, *ApJS*, 208, 19
- Jarosik, N., Barnes, C., Greason, M. R., et al. 2007, *ApJS*, 170, 263
- Joshi, N., Das, S., Rotti, A., Mitra, S., & Souradeep, T. 2012, arXiv:1210.7318
- M. A. J. Ashdown, C. Baccigalupi, A. Balbi, et al. 2007, *A&A*, 467, 761
- Mitra, S., Rocha, G., Górski, K. M., et al. 2011, *ApJS*, 193, 5
- Mitra, S., Sengupta, A. S., Ray, S., Saha, R., & Souradeep, T. 2009, *MNRAS*, 394, 1419
- Mitra, S., Sengupta, A. S., & Souradeep, T. 2004, *Phys. Rev. D*, 70, 103002
- Moss, A., Scott, D., & Sigurdson, K. 2011, *J. Cosmology Astropart. Phys.*, 1, 1
- Planck Collaboration, Ade, P. A. R., Aghanim, N., et al. 2013a, arXiv:1303.5076
- . 2013b, arXiv:1303.5083
- . 2013c, arXiv:1303.5084
- Pullen, A. R., & Kamionkowski, M. 2007, *Physical Review D*, 76, 103529
- Rotti, A., Aich, M., & Souradeep, T. 2011, arXiv:1111.3357
- Souradeep, T., Mitra, S., Sengupta, A., Ray, S., & Saha, R. 2006, *New A Rev.*, 50, 1030
- Souradeep, T., & Ratra, B. 2001, *ApJ*, 560, 28
- Tegmark, M., de Oliveira-Costa, A., & Hamilton, A. J. S. 2003, *Phys. Rev. D*, 68, 123523

---

This 2-column preprint was prepared with the AAS L<sup>A</sup>T<sub>E</sub>X macros v5.2.